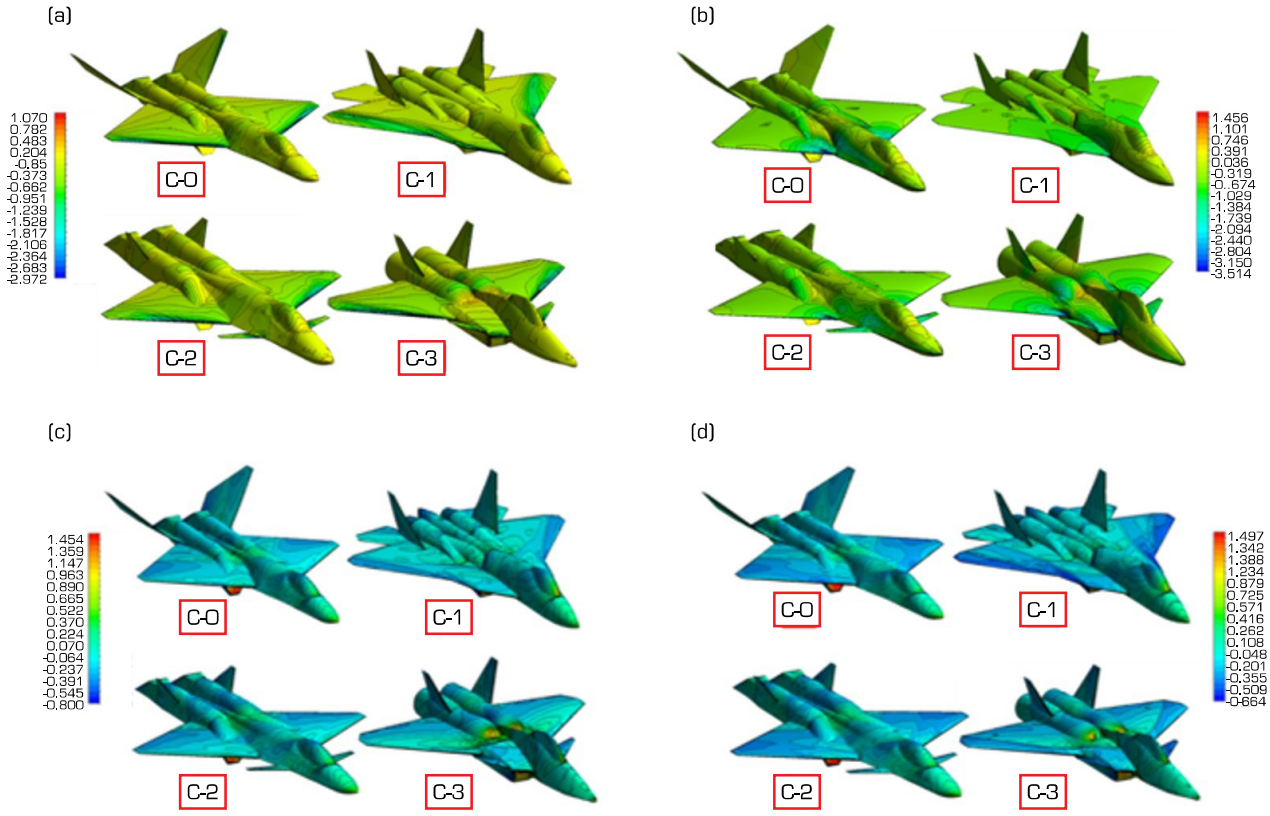

Figure 13. Comparison of Pressure coefficient at subsonic and supersonic Mach. (a) Subsonic 8° AOA; (b) Subsonic 24° AOA; (c) Supersonic 2° AOA; (d) Supersonic 6° AOA;

The shock waves are generated over the aircraft surface as flow becomes sonic, that is, M ≥ 1.0. The primary implication of this shock is an increase in the static pressure of the air. This can be seen from the color legends in supersonic regime as the absolute value of negative pressure is dropped from 3 to 0.7. Figure 13 also presents the pressure distribution at supersonic speed at Mach 1.4 and 2° AoA. The most impressive C_p distribution over the leading edge is observed in C-1 configuration. A large negative pressure can be seen over the wing surfaces of C-2 and C-3 configurations. The effect of poorly shaped blended nacelle is drastic at supersonic velocity as the flow is largely affected span wise over the C-3 wing. Concept-0 wing also has appreciable lift distribution over the surface. Canard of C-3 has a larger sweep angle as compared to C-2 and thus appears to be more effective at supersonic speeds. Due to the formation of shock waves, a high pressure can also be seen over the leading edges of V-tail surface, that is, smoothened out as the flow moves downstream the surface. Large region of relative high pressure can also be seen over the V-tail of C-0 configuration. One of the notable features in C-3 configuration is the shape of its nose surface, which results in improved C_p distribution. At supersonic state at 6° AOA, it is evident that C-1 has the best pressure distribution across the leading edges, followed by C-3 configuration. Meanwhile, it is also improved on the leading edges of other configurations as well. Concept-1 has the best canopy shape due to its sleek design, the same was observed for all flight conditions. Moreover, C-1 appears to have the best exhaust design in terms of aerodynamic efficiency, as compared to other configurations for all simulated flight conditions. However, due to a sharp fairing and shock wave interaction, a slight high-pressure region can be observed in the mid fuselage section just ahead of blended engine nacelle. Regions of high pressure can also be seen in the mid fuselage region for different aircraft. The pressure distribution is slightly improved on the V-tail of C-0 aircraft. Concept-0 and C-2 have the highest pressure at the engine inlets, while the lowest is seen on the C-1 configuration.

The eddies are the swirling of fluid that are generated when a turbulent flow passes an obstacle in its path. An eddy is not a property of fluid, but a violent swirling motion caused by the position and direction of turbulent flow. The eddy viscosity is the proportionality factor describing the turbulent transfer of energy as a result of moving eddies, thus giving rise to tangential stresses.

At 10° AoA, the small eddies are seen on the wing tips, indicating downwash from the wing. The eddies can also be seen on the downstream of the engine exhaust. As the AoA is increased, the magnitude of vortex shedding is also especially increased, which is visible in Fig. 14. At post-stall AoA, there is a decrement in the magnitude of eddy viscosity, primarily due to flow separation. At 50°, it is clear that the flow is separated completely from the surface of the aircraft.

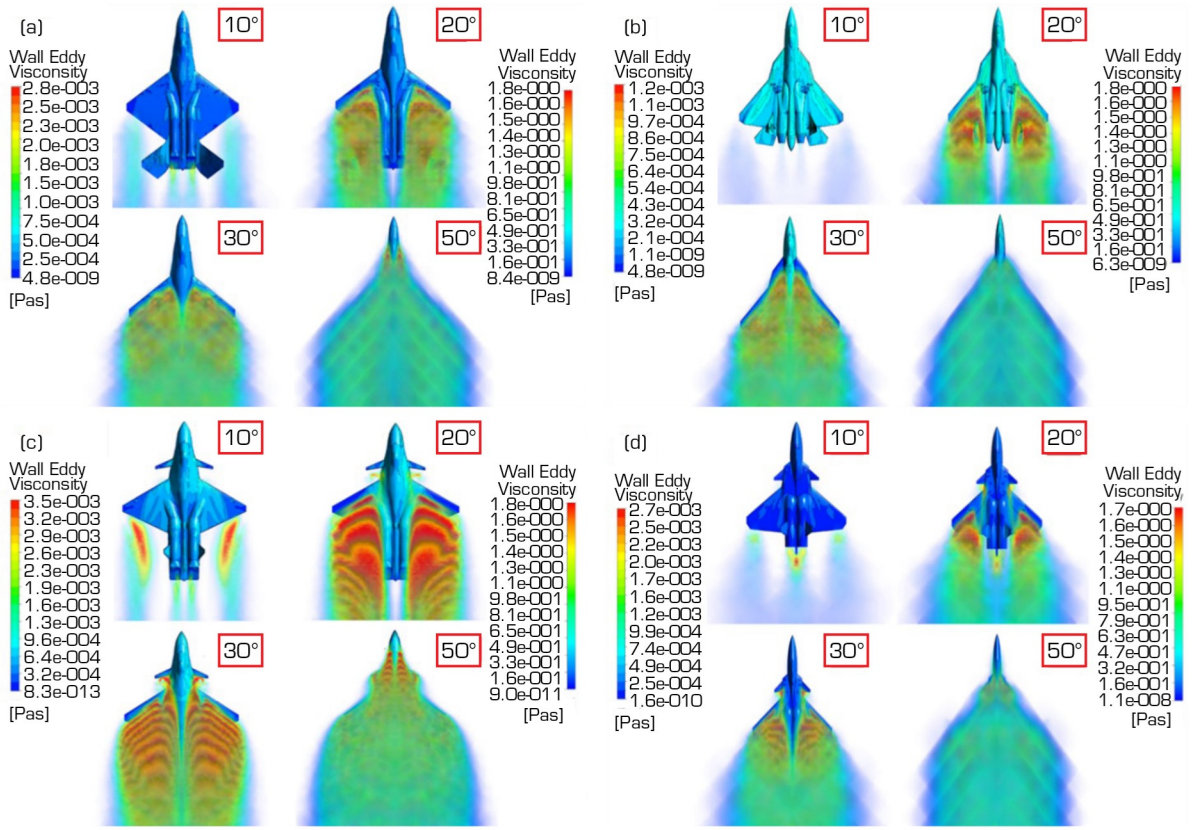

Figure 14. Visualization of eddy viscosity at various AoA. (a) Concept-0; (b) Concept-1; (c) Concept-2; (d) Concept-3.

Concept-1 is found to have smallest eddies shedding from the wingtips at 10° AoA as compared to other configurations. The eddies are somewhat delayed and found to be emitting from the mid-chord wing surface at 20° AoA. However, they are strong in magnitude and strongly affect the flow over the vertical tail. In the post-stall regime, Fig. 14 indicates the interaction among the vortices, especially in the reattachment of secondary wingtip vortices. At 50°, the aircraft appears to be stalled completely.

Concept-2 appeared to shed the strongest eddies than all other configurations. In Fig. 14, the strong eddies can be seen shedding from the wingtips at 10° AoA. As the AoA is increased to 20° AoA, the flow eddies grow in size and strength, producing at a location near to the quarter-chord of the wing. At 30°, the strength of eddy viscosity is somewhat reduced, except in the canard region, mainly due to the flow separation. At 50°, the strength of eddy viscosity is dissipated, except in the canard section.

The eddy viscosity is high at 10° AoA as compared to the other configurations, particularly in the engine exhaust region. The stronger eddies appear on the wing surface in the mid-chord region at 20° AoA. The eddies become stronger as they travel along the surface and diminishes when moving away. Figure 14 shows that the 30° is the post-stall regime as strength of eddies is decreased due to separation. At 50°, the flow appears to be separated completely on the aircraft, except on the nose section.

The flow topologies of the configurations at different AoA are illustrated by a common iso-value of Q-criterion in Fig. 15. Q-criterion is a flow visualization tool that highlights the vortex-based areas where the magnitude of the vorticity tensor (Ω) exceeds the magnitude of the strain rate tensor (S) and is expressed by Eq. 2:

$$Q = \frac{1}{2}(\|\Omega\|^2 - \|S\|^2) \tag{2}$$

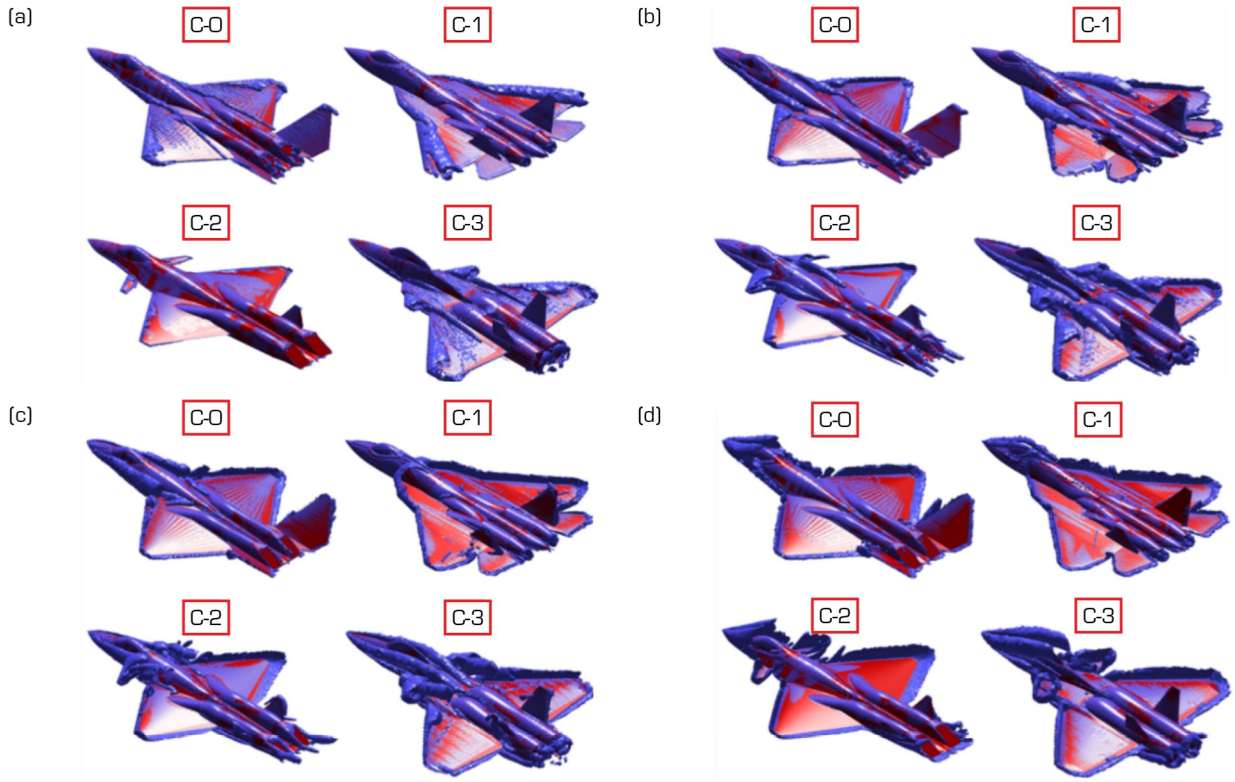

Figure 15. Visualization of the vortex core at a common value of Q criterion at various flow angles. (a) 10° AOA; (b) 20° AOA; (c) 30° AOA; (d) 50° AOA.

From the figure, the major contribution of vortex generation at low to moderate AoA can be observed due to the pressure difference between upper and lower surfaces of the wing. The formation of forebody vortices, canard vortices and the wing tip and leading edges vortices majorly affects the aerodynamics of the configurations. At 10° AoA (refer Fig. 15), the vortices of significant magnitude appear on the upper surfaces of C-1 and C-3. Concept-1 vortices are mainly due to its delta wing configuration, but are restricted to the wing tips only. The flow near the root chord of the wing seems to be unaffected as the flow moves along the surface. However, the vortices on C-3 indicate that it is disturbing the air flow on the surface of the wing because of canard surfaces. Concept-0 and C-2 have smaller magnitude of vortices mainly on the edges of the surfaces. Concept-2 has the minimum magnitude of vortices.

From Fig. 15, it can be observed that the vortices on the C-0 and C-2 remain small and restricted as compared to C-1 and C-3 at 20° AoA. However, canard of C-2 appears to be significantly affected by the vortices. Reynolds-averaged Navier–Stokes simulation has captured the interaction of canard, forebody and wing vortices in C-2 and C-3. Vortex core generated by the nose of the aircraft C-0 and C-2 moves downstream and ends near the quarter chord of the wing root. Concept-3 again has the largest magnitude of vortices. The vortices formed at the nose are larger in magnitude as compared to all other configurations. The vortices formed near the canard severely affect the canard surfaces and remain significant until the mid-chord of the wing root. The wing surface is also affected by the vortices, mainly at the leading edge, especially near the mean aerodynamic chord. There are no significant vortices near the nose of the C-1 aircraft even at 20° AoA. The vortices are significant only at the leading edges of the front delta and weaken as it approaches to the quarter chord of the wing root. The vortices also diminishes as they travel downstream along the leading edges of the wing. The horizontal stabilizer is slightly affected by the vortices. The vortices also appear only on the junction of wing vertical tail, but they are smaller in magnitude due to small pressure difference.

At the post-stall AoA (50°), it can be observed that C-1 is relatively less affected by the vortices than the other configurations. Concept-0 and C-2 have similar planforms and nose-shape, yet the effect of vortices is larger on C-2, especially in the trailing edge of wing. Canard surfaces of C-2 and C-3 are extremely affected at this AoA. Concept-1 has a remarkable nose shape as the vortices are very low in magnitude, even at the post-stall AoA. There are significant vortices at the front delta wing, suggesting to be completely affected. At a very high AoA, Fig. 15 indicates that excessive vortices are formed in the nose region of C-0, C-2 and C-3 configuration with the highest for C-3. Concept-0 has

less vortices along the edges of its wing as compared to other configurations, but still, they are substantial. The flow around the nose is found to be better for C-1 configuration due to its superior nose shape, yet, due to delta wing configuration, the wing is largely affected by the wing tip vortices. Concept-3 nose shape does not appear to be optimal, as it is generating larger region of vortices that indicates more drag.

Leading-Edge Suction Analogy-Based Vortex Lift Estimation

Based on the vortex lift concept using leading edge suction analogy, an empirical study is conducted for estimating the lift coefficient for delta wings at low AoA. The mathematical formulation of Polhamus method is expressed in Eq. 3:

$$C_L = K_P \sin\alpha \cos^2\alpha + K_v \cos\alpha \sin^2\alpha \tag{3}$$

where K_p and K_v are proportionality constant for potential and vortex lift. K_p is dependent on the wing aspect ratio. On the contrary, the value K_v is nearly constant and is usually taken as π.

The subject models have triangular wings with aspect ratios ranging from 2 to 2.6. Therefore, the force constants are evaluated through Eqs. 4 and 5, presented by Maybury *et al.* (2001):

$$K_P = 1.393AR - 0.141AR^2 \tag{4}$$

$$K_v = 3.157 - 0.020AR + 0.021\,AR^2 \tag{5}$$

where AR represents the aspect ratio. The values of these constants are presented in Table 4 for each concept.

Table 4. Lift proportionality constants.

Concept-0		Concept-1		Concept-3	
AR	2.0030	AR	2.3113	AR	2.5215
K_p	2.2245	K_p	2.4664	K_p	2.6160
K_v	3.2012	K_v	3.2230	K_v	3.2401

The plots of the analytical and numerically computed value of the wing lift coefficients are depicted in Fig. 16 for each configuration. Among the given aircraft configuration, C-1 wing resembles the delta wing configuration and it can be observed from Fig. 16 that numerically calculated lift coefficient follows the analytical estimate curve closely for the given values of K_p and K_v.

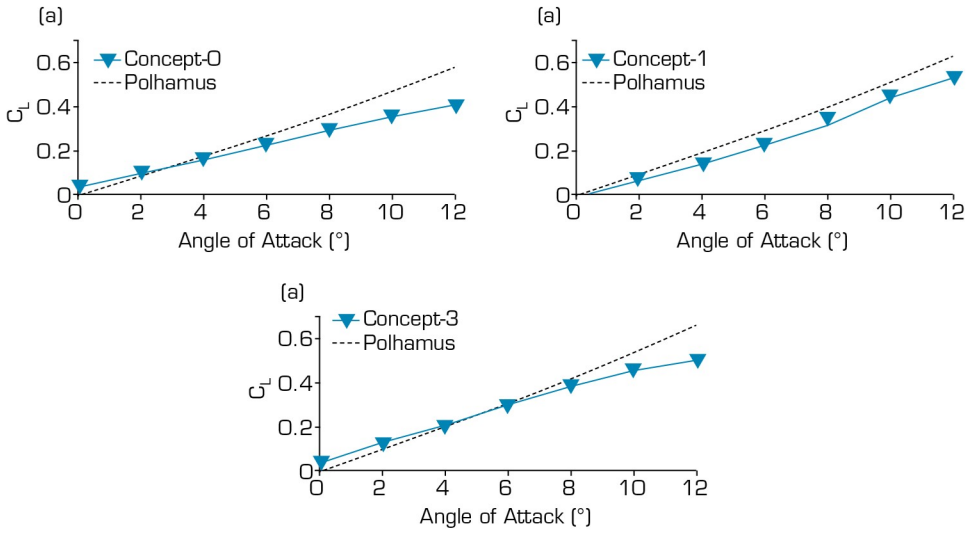

Figure 16. Comparison of analytical and numerical lift coefficient. (a) Concept-0; (b) Concept-1; (c) Concept-3.

Post-Stall Estimation of Lift Coefficient

The numerical results are achieved till 60°, after which the solution largely oscillates and diverges. To predict the further behavior of the lift coefficient with variation in AoA, the curve fitting techniques were highlighted by Duquette (2007). Among these techniques, Duquette suggested the post-stall method by Viterra and Corrigan for accurate estimation of C_L between the stall angle (α_{stall}) and 90°. Therefore, the method was implemented in the current research work, and Eqs. 6, 7, 8 and 9, presented in the research by Duquette (2007), were used.

$$C_L = A1 sin2\alpha + \frac{A2 cos^2\alpha}{sin\alpha} \tag{6}$$

$$A1 = \frac{C_{D,MAX}}{2} \tag{7}$$

$$A2 = \left(C_{L,stall} - C_{D,MAX} * sin\alpha_{stall} * cos\alpha_{stall}\right) \frac{sin\alpha_{stall}}{cos^2\alpha_{stall}} \tag{8}$$

$$C_{D,MAX} = 1.11 + 0.018AR \tag{9}$$

Based on these formulations, Eqs. 10, 11, 12 and 13 were derived for the conceptual aircraft.

$$C_L = 0.57303 sin2\alpha + \frac{0.97924 cos^2\alpha}{sin\alpha}; (C\ 0) \tag{10}$$

$$C_L = 0.57580 sin2\alpha + \frac{0.91607 cos^2\alpha}{sin\alpha}; (C\ 1) \tag{11}$$

$$C_L = 0.57758 sin2\alpha + \frac{0.96336 cos^2\alpha}{sin\alpha}; (C\ 2) \tag{12}$$

$$C_L = 0.57770 sin2\alpha + \frac{0.94573 cos^2\alpha}{sin\alpha}; (C\ 3) \tag{13}$$

It is notable to mention that these equations are applicable for the angles beyond 60°. The behavior of lift coefficient between the angles –10 and 90° are presented in Fig. 17 for each configuration. This data is useful for modeling agile maneuvers of Advanced Tactical Fighter (ATF) for performance analysis and studying complex trajectories, such as cobra maneuvers.

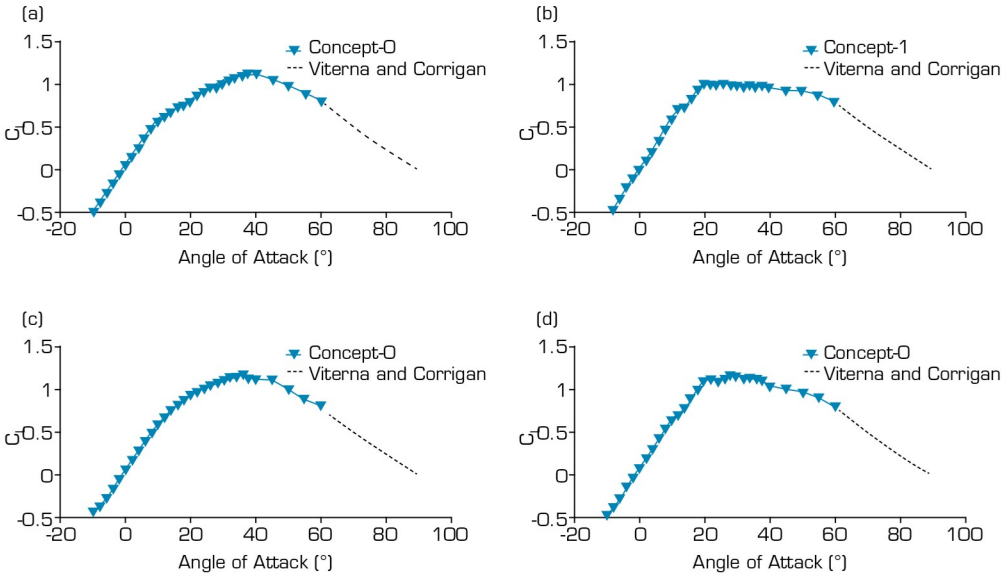

Figure 17. Lift coefficient trend based on CFD runs and post-stall method.
(a) Concept-0; (b) Concept-1; (c) Concept-2; (d) Concept-3.

Contribution of Components

Fuselage

Figure 18 shows the fuselage contribution towards lift, drag and lift-to-drag ratio at different AoA at a subsonic Mach No. of 0.6. Due to fairing on the C-0 configuration, lift on the fuselage region is found to be more as compared to other configurations. However, the drag encountered by it is also higher as compared to the other configuration at near and beyond stall AoA. This suggests an improvement in the geometry shape of fuselage in order to attain less drag and consequently a higher L/D ratio.

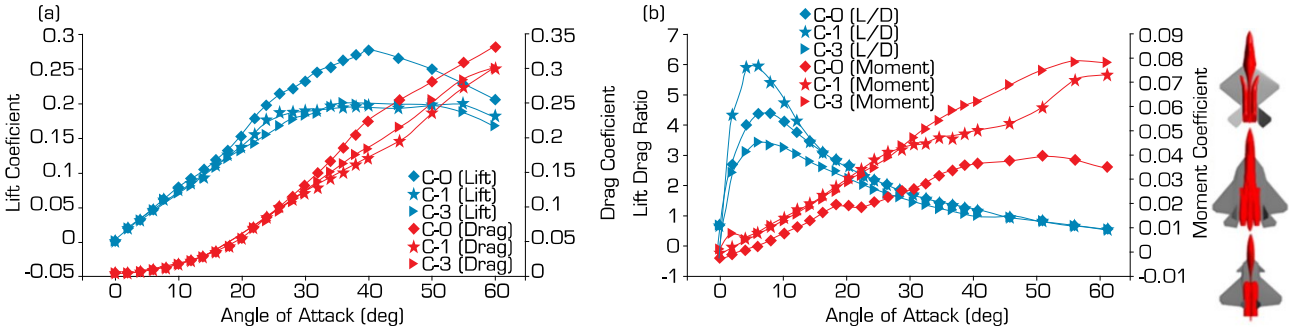

Figure 18. Aerodynamic contributions of Fuselage at Subsonic Mach. (a) Contribution in overall lift and drag. (b) Contribution in lift-to-drag ratio and pitching moment.

Concept-1 configuration has nominal lift at all AoA and has a relative less amount of drag. Better fairing on the surface and streamlined shape of the fuselage resulted in the highest L/D among other configurations. Concept-3 has generated less lift due to the high-pressure region generated in the mid-fuselage section ahead of fairing. This has affected the aerodynamic performance, as L/D is lower for C-3 at all AoA before stall.

Wing

The primary function of a wing is to generate sufficient lift in order to sustain flight and thus the most important component of an aircraft. The wing planform is the shape of the wing viewed directly from the above, coming in different configurations with each having its own advantages and disadvantages. Figure 19 compares the aerodynamic characteristics w.r.t AoA of the wing of different aircraft configurations in subsonic flight of Mach 0.6. Concept-0 configuration consist of a trapezoidal wing with a significant taper-ratio. The lift coefficient is found to be less than other aircraft at all AoA. However, as this configuration is much closer to the ideal elliptical wing, the drag coefficient is less than other aircraft, and lift-to-drag (L/D) ratio was highest for C-0 configuration. Concept-0 configuration is marginally unstable as coefficient of moment increases slowly with AoA before stall. However, beyond stall it is found to be fairly stable. The stall is achieved at moderate AoA. After stall, the flow is found to remain attached only in the small portion of leading edge at 30° AoA. At 50°, the flow is completely detached from the upper surface of the wing, leaving a large separation region suggesting a high pressure drag.

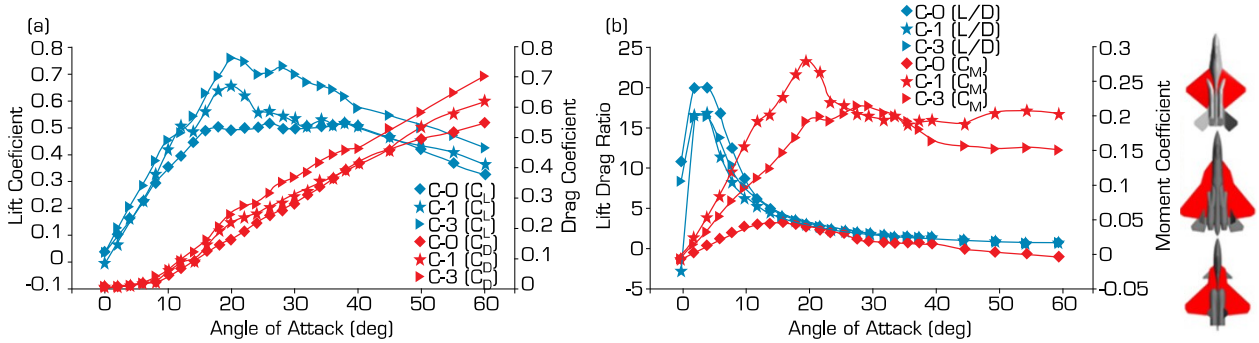

Figure 19. Aerodynamic contributions of Wing at Subsonic Mach. (a) Contribution in overall lift and drag. (b) Contribution in lift-to-drag ratio and pitching moment.

In C-1 configuration, the wing planform is double-delta with sweep forward trailing edge. Lift coefficient is found to be more than C-0 configuration with relative higher drag. However, due to its delta wing configuration, stall is delayed to nearly 20° AoA. As there is a rapid decrease in the lift coefficient, the post-stall effect is found to be dramatic. The lift-to-drag ratio is low at low AoA; however, it is improved as the AoA is increased and was found slightly higher than C-3. It can also be seen that the wing of C-1 configuration is the most unstable configuration from the moment coefficient curve. Cm increases almost linearly with the AoA and results in higher slope than other configurations.

Concept-3 is a cropped delta wing aircraft. The lift coefficient is found higher for C-3 than all the other configurations throughout all AoA. However, the coefficient of drag can be observed to be higher as well. This decreases the overall aerodynamic performance of the wing as lift-to-drag ratio is not as impressive as C-0, but it is similar to C-1. The stall angle is slightly higher than C-1. Concept-3 wing is also unstable; however, the behavior is benign relative to C-1.

Vertical Tail

The tail in C-0 is in the form of V-tail with large surface region. In Fig. 20, the coefficient of lift is the highest, suggesting large nose-down moment being generated by the tail. This is true only till moderate AoA. The lift coefficient drops exponentially as the AoA is increased from 8° and remains very low till 25°, signifying the inefficiency of tail in between these AoA. Since there is no horizontal stabilizer, a negative lift coefficient that can be seen in Fig. 20 further indicates a destabilizing nose-up moment being generated, which can also be seen in the right figure as an increase in the coefficient of moment. The lift-to-drag ratio is notable at low AoA. However, there is a sudden drop in L/D ratio as the AoA is in 20–25° range. Concept-1 has twin vertical tail, which is inclined at very small angle. The coefficient of lift is very small and slightly increases with the AoA. Nonetheless, it starts dropping at nearly 15° AoA. In the post-stall regime, the coefficient of lift remains nearly constant throughout showing stabilizing effect on the aircraft. The coefficient of moment is marginally negative throughout all the AoA.

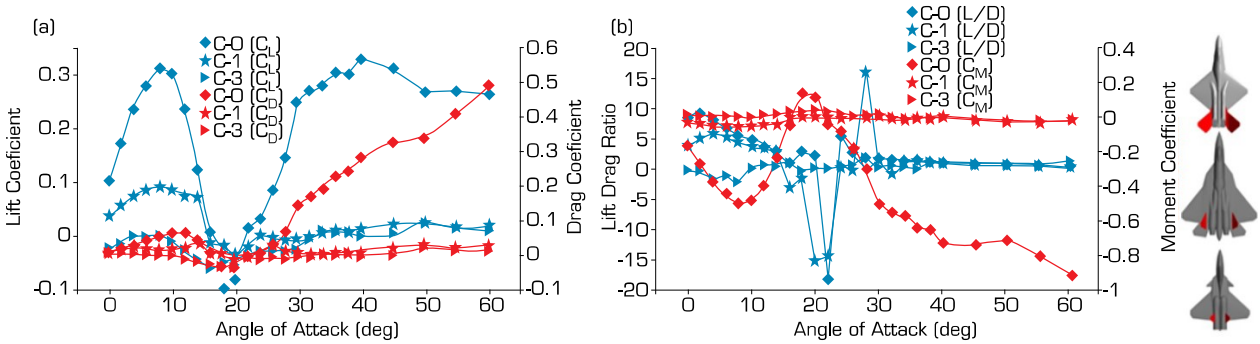

Figure 20. Aerodynamic contributions of Vertical tail at Subsonic Mach. (a) Contribution in overall lift and drag. (b) Contribution in lift-to-drag ratio and pitching moment.

The lift-to-drag ratio is impressive only at small AoA. There is a drop in L/D ratio to negative values as the AoA is between 15–25° range. There is a V-tail configuration in C-3 configuration, which is smaller in size. There is no horizontal stabilizer present in the aircraft. The lift-coefficient is small and mostly negative before stall. The coefficient of moment is slightly negative throughout all AoA. The lift-to-drag ratio shows poor aerodynamic efficiency of the vertical tail with highest value of 2~2.5. Overall, the lift-to-drag ratio is not impressive at all AoA, which indicates the need for modification in the design of V-tail of the C-3 aircraft.

Canard/Horizontal Tail

Figure 21 depicts the aerodynamic characteristics of horizontal surfaces of C-1 and C-3 configurations. A sweepback canard is present in C-3 configuration ahead of the wing. Canards are located ahead of the CG intentionally in order to destabilize the aircraft for greater maneuverability, especially at high AoA. From the $C_{L\text{-}\alpha}$ curve, the canard is seen to be generating lift efficiently till 30° AoA. As the angle is increased from 30°, the lift coefficient starts to drop, suggesting it to be stalled. The lift-to-drag ratio is very high at low AoA, reaching a value of 28 before dropping at moderate AoA. The canards are found to have positive moment

coefficient through all the AoA. The horizontal tail is present in C-1 configuration only just aft of the wing. The primary role of the horizontal tail is to provide longitudinal stability to the aircraft. At low AoA, the lift coefficient of horizontal tail is not notable, thus indicating poor performance at those angles. At moderate to high AoA, there is a sudden increase in the lift coefficient before retaining a nearly constant value. Moment coefficient is found to be very small and slightly negative at moderate-high AoA. The lift-to-drag ratio is not very impressive as well. A redesign of the horizontal stabilizer is suggested to ensure better performance under vortex shedding from the wing.

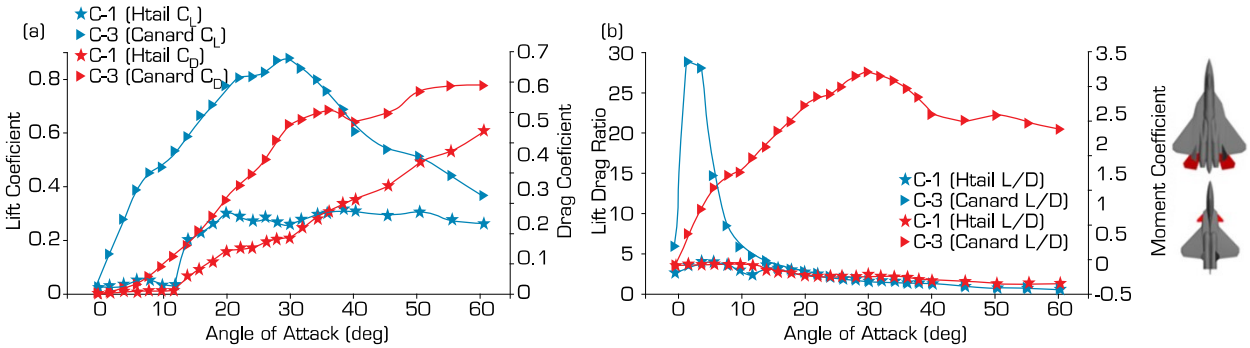

Figure 21. Aerodynamic contributions of Horizontal Tail / Canard at Subsonic Mach. (a) Contribution in overall lift and drag. (b) Contribution in lift-to-drag ratio and pitching moment.

CONCLUSION

Computational fluid dynamics is known to be a very useful tool in the aerodynamic analysis of aircraft. It not only provides deep information about the flow, which helps in the design optimization, but is also very cost-effective as compared to experimental techniques. However, for complex analyses, computational cost increases exponentially, yet significant less than wind tunnel operational cost.

Due to the unavailability of aerodynamic data on the fighter aircraft at different Mach numbers, CFD model was validated against ONERA M6 wing and UCAV SACCON, which provides fairly accurate results for 3D flows. However, many complex flow phenomena, like interaction of downstream vortices with the surface, post-stall aerodynamics, interference etc., need better benchmark for the CFD validation. In order to gain confidence in the CFD model, mesh sensitivity is checked and tight convergence criteria is employed in order to have minimum numerical errors. Computational fluid dynamics analysis provides key aerodynamic performance and stability parameters about the four conceptual designs (C-0, C-1, C-2 and C-3).

The comparison of aerodynamic performance parameter, which is a ratio of the lift-to-drag (L/D) of different aircraft in subsonic and supersonic flight regimes, has been studied and presented in this study. The highest wave drag is observed for the configuration C-0 wing to the abrupt changes in area distribution. However, the latter concept is the only among the four models symbolizing a positive static margin based on the CG location. Concept-1 performs the best in terms of drag behavior and lift to drag ratio in both flow regimes. Additionally, the highest supersonic lift and drag are observed in the configuration C-2. In subsonic regime, all configurations are longitudinally statically unstable. By carefully analyzing the shift of neutral point in moving from subsonic to supersonic flight regime, the aircraft becomes more statically stable. Also, each configuration exhibits flat surface behavior of C_L at very high AoA.

Furthermore, the areas in which improvements can be made in order to further enhance its flight capability were also identified from the flow visualization over the four aircraft. It is highly recommended to add engine fairing in C-3 concept and repositioning of its canard surface, so that the effects of vortices on the wings are minimized. The reshaping of the canopy should also be considered. Concept-1 fuselage appears to have slightly better aerodynamic features, as it shows higher values of L/D at normal flying AoA. Concept-1 seems to have lowest drag in the supersonic regime, yet it is recommended to redesign blended engine nacelle. The features that are suggested to be improved in C-0 are wing leading edge, engine nacelle fairing and vertical tail.

AUTHORS' CONTRIBUTION

Conceptualization: Siddiqui W, Maqsood A, Riaz R, Salamat S; **Methodology:** Siddiqui W, Zahid M.S, Naseer H, Maqsood A; **Investigation:** Siddiqui W, Zahid M.S, Naseer H; **Writing – Original Draft:** Siddiqui W and Maqsood A; **Writing – Review and Editing:** Siddiqui W and Maqsood A; **Supervision:** Maqsood A, Riaz R and Salamat S.

DATA AVAILABILITY STATEMENT

All the datasets were generated and analyzed during the current study.

FUNDING

Not applicable.

ACKNOWLEDGEMENTS

The authors would like to extend their sincere thanks to the supercomputing facility at Research Center for Modelling and Simulation for their technical support.

REFERENCES

Abney E, McDaniel M (2005) High Angle of Attack Aerodynamic Predictions Using Missile Datcom. Paper presented 23rd AIAA Applied Aerodynamics Conference. AIAA; Toronto, Ontario, Canada. https://doi.org/10.2514/6.2005-5086

Amadori K, Jouannet C, Krus P (2008) Aircraft Conceptual Design Optimization. Paper presented ICAS 26th International Congress of the Aeronautical Sciences.

Sutrisno S, Wibowo SB, Iswahyudi S, Rohmat TA (2019) Rolled-Up Vortex Dynamic Numerical Studies of Bird's-Body-Type Fighter. Int J Mech Eng Technol 10(3):304-316.

Bitencourt LO, Pogorzelski G, Freitas RM, Azevedo JLF (2011) A CFD-based analysis of the 14-Bis aircraft aerodynamics and stability. J Aerosp Technol Manag 3(2):137-146. https://doi.org/10.5028/jatm.2011.03021711

Blake W (1985) Prediction of fighter aircraft dynamic derivatives using Digital Datcom. Paper presented 3rd Applied Aerodynamics Conference. AIAA; Colorado Springs, Colorado, United States. https://doi.org/10.2514/6.1985-4070

Boelens OJ (2012) CFD analysis of the flow around the X-31 aircraft at high angle of attack. Aerosp Sci Technol 20(1):38-51. https://doi.org/10.1016/j.ast.2012.03.003

Della Vecchia P, Ciliberti D (2013) Numerical aerodynamic analysis on a trapezoidal wing with high lift devices: a comparison with experimental data. Paper presented XXII AIDAA Conference. AIDAA; Naples, Italy.

Duquette M (2007) Development and Application of SimpleFlight, a Variable-Fidelity Flight Dynamics Model. Paper presented AIAA Modeling and Simulation Technologies Conference and Exhibit. AIAA; Hilton Head, South Carolina, United States. https://doi.org/10.2514/6.2007-6372

ANSYS Inc (2017) ANSYS Fluent Theory Guide. Release 18.0. ANSYS Inc.

Kostić IA, Stefanović ZA, Kostić OP (2014) Aerodynamic analysis of a light aircraft at different design stages. FME Trans 42:94-105.

Kryvokhatko IS, Masko OM (2017) Aerodynamic Characteristics and Longitudinal Stability of Tube Launched Tandem-Scheme UAV. In Volkov K, editor. Flight Physics: Models, Techniques and Technologies. London: IntechOpen. p. 73-83.

Loeser T, Vicroy D, Schuette A (2010) SACCON Static Wind Tunnel Tests at DNW-NWB and 14´x22´ NASA LaRC. Paper presented 28th AIAA Applied Aerodynamics Conference. AIAA; Chicago, Illinois, United States. https://doi.org/10.2514/6.2010-4393

López D, Domínguez D, Gonzalo J (2013) Impact of turbulence modelling on external supersonic flow field simulations in rocket aerodynamics. Int J Comut Fluid Dyn 27(8-10):332-341. https://doi.org/10.1080/10618562.2013.867951

Mason W, Knill D, Giunta A, Grossman B, Watson L, Haftka R (1998) Getting the full benefits of CFD in conceptual design. Paper presented 16th AIAA Applied Aerodynamics Conference. AIAA; New Mexico, United States. https://doi.org/10.2514/6.1998-2513

Maybury WJ, Rayner JMV, Couldrick LB (2001) Lift generation by the avian tail. Proc R Soc Lond B Biol Sci 268(1475):1443-1448. https://doi.org/10.1098/rspb.2001.1666

Menter FR (1994) Two-equation eddy-viscosity turbulence models for engineering applications. AIAA J 32(8):1598-1605. https://doi.org/10.2514/3.12149

Nelson RC (1998) Flight Stability and Automatic Control. New York: McGraw-Hill Education.

Nicolosi F, Della Vecchia P, Ciliberti D, Cusati V (2014) Development of new preliminary design methodologies for regional turboprop aircraft by CFD analyses. 29th Congress of the International Council of the Aeronautical Sciences. St. Petersburg, Russia.

Schminder J (2012) Feasibility study of different methods for the use in aircraft conceptual design. Linköpings (Thesis). Linköpings Universitetet. In english.

Schmitt V, Charpin F (1979) Pressure Distributions on the ONERA M6-Wing at Transonic Mach Numbers. In AGARD, editor. Experimental Data Base for Computer Program Assessment. Seine: AGARD.

Schütte A, Cummings RM, Loeser T, Vicroy DD (2009) Integrated Computational/Experimental Approach to UCAV and Delta-Canard Configurations Regarding Stability & Control. Paper presented 4th Symposium on Integrating CFD and Experiments in Aerodynamic. Brüssel, Belgien.

Spalart P, Allmaras S (1992) A one-equation turbulence model for aerodynamic flows. Paper presented 30th Aerospace Sciences Meeting and Exhibit. AIAA; Reno, Nevada, United States. https://doi.org/10.2514/6.1992-439

Tinoco EN (1991) CFD codes and applications at Boeing. Sadhana 16(Part 2):141-163. https://doi.org/10.1007/BF02812178

Tseng JB, Lan CE (1988) Calculation of Aerodynamic Characteristics of Airplane configurations at High Angles of Attack. Washington: NASA.

Wibowo SB, Sutrisno I, Rohmat TA (2018) An Evaluation of Turbulence Model for Vortex Breakdown Detection Over Delta Wing. Arch Mech Eng 65(3):399-415.

Williams JE, Vukelich SR (1979) The USAF Stability and Control Digital DATCOM. Volume I, Users Manual. St. Louis: McDouglas Astronautics Company.

Xue RR, Ye ZY, Wang G (2016) Aerodynamic Characteristic Comparison of the Forward and Backward-Swept Wings. Paper presented 30th Congress of the International Council of the Aeronautical Sciences. ICAS; Daejeon, Korea.

Zhong Y, Zhao K (2012) Cfd-based research of strake effects for low speed high lift configuration. Paper presented 28th International Congress of the Aeronautical Sciences. ICAS; Brisbane, Australia.